



Force sensors for measuring microenvironmental forces during mesenchymal condensation

Robert A. Gutierrez^a, Wenqiang Fang^b, Haneesh Kesari^{b,**}, Eric M. Darling^{a,b,c,d,*}

^a Center for Biomedical Engineering, Brown University, Providence, RI, 02912, USA

^b School of Engineering, Brown University, Providence, RI, 02912, USA

^c Department of Molecular Pharmacology, Physiology, and Biotechnology, Brown University, Providence, RI, 02912, USA

^d Department of Orthopaedics, Brown University, Providence, RI, 02912, USA

ARTICLE INFO

Keywords:

Cell mechanics
Traction force microscopy
Elasticity
Morphogenesis
Microtissues
Self-assembly

ABSTRACT

Mechanical forces are an essential element to early tissue formation. However, few techniques exist that can quantify the mechanical microenvironment present within cell-dense neotissues and organoid structures. Here is a versatile approach to measure microscale, cellular forces during mesenchymal condensation using specially tailored, hyper-compliant microparticles (HCMPs). Through monitoring of HCMP deformation over both space and time, measurements of the mechanical forces that cells exert, and have exerted on them, during tissue formation are acquired. The current study uses this technology to track changes in the mechanical microenvironment as mesenchymal stem cells self-assemble into spheroids and condense into cohesive units. An array analysis approach, using a high-content imaging system, shows that cells exert a wide range of tensile and compressive forces during the first few hours of self-assembly, followed by a period of relative equilibrium. Cellular interactions with HCMPs are further examined by applying collagen coating, which allows for increased tensile forces to be exerted compared to non-coated HCMPs. Importantly, the hyper-compliant nature of our force sensors allows for increased precision over less compliant versions of the same particle. This sensitivity resolves small changes in the microenvironment even at the earliest stages of development and morphogenesis. The overall experimental platform provides a versatile means for measuring direct and indirect spatiotemporal forces in cell-dense biological systems.

1. Introduction

Mechanical forces generated by cells are critical for regulating many biological phenomena, including tissue assembly and morphogenesis [1–3]. Measuring these forces in cell-dense tissues has been a challenge due to the lack of physical tools that can be inserted into a biological system without dramatically influencing its structure and behavior. Existing methods to investigate cellular forces include traction force microscopy (TFM) [4,5] and micropillars [6], which work well for studying cells in isolation but are poorly suited for cell-dense structures since they require a mechanically well-defined bulk material that contains fiducial markers for deformation tracking. Furthermore, these techniques are typically implemented in two-dimensions (2D) and are difficult to translate into three dimensional (3D) culture environments, which are more physiologically relevant for many biological systems [7].

As an alternative to bulk material deformation tracking, oil microdroplets and deformable microparticles (MPs) have recently been used as *in situ* force sensors to measure cell-generated forces in highly cellular tissue structures [8–13]. To date, these investigations have focused primarily on general observations of forces in tissue peripheries or cell layer cultures [8,10,12], using MPs with elasticity >1 kPa, which inherently limits measurement accuracy and sensitivity. Previous work using lower elasticity materials has been done using large MPs (>50 μm diameter), which greatly exceeds the typical size of individual cells [11]. The characteristics of cell-generated forces during tissue assembly remains unknown and has yet to be quantitatively described for the earliest stages of this fundamental process.

The goal of this study was to quantify microenvironmental forces during mesenchymal condensation in a spheroid model system by using a parallelized *in situ* force sensor platform. To achieve this, we developed

* Corresponding author. Center for Biomedical Engineering, Brown University, Providence, RI, 02912, USA.

** Corresponding author. 184 Hope St, Providence, RI, 02912, USA.

E-mail addresses: haneesh kesari@brown.edu (H. Kesari), eric_darling@brown.edu (E.M. Darling).

<https://doi.org/10.1016/j.biomaterials.2021.120684>

Received 19 August 2020; Received in revised form 12 January 2021; Accepted 13 January 2021

Available online 20 January 2021

0142-9612/© 2021 Elsevier Ltd. All rights reserved.

a platform methodology for making repeated, non-destructive measurements of microenvironmental pressure and elastic energy density in 3D by including mechanically uniform MPs alongside mesenchymal stem cells as they self-assemble into neotissues. We initially created our custom MPs via an inverse emulsion process to form hyper-compliant microparticles (HCMPs) from polyacrylamide, chosen due to its tunable mechanics, biocompatibility, and surface functionalization to facilitate cell adhesion [14–16]. HCMPs were made with an elastic modulus of 0.26 ± 0.04 kPa, (4% acrylamide, 0.5% bis-acrylamide) and diameters ranging from 15 to 45 μm (Fig. S1). They were fluorescently stained to allow 3D imaging of deformation over time, and surfaces were either kept non-coated or coated with covalently bound collagen type I to distinguish between direct and indirect cell-HCMP interactions and forces. Human adipose-derived stem cells (ASCs) were selected as the cell type of interest since they can differentiate into all mesodermal lineages and undergo mesenchymal condensation when placed in non-adhesive microwells [17–19]. This study tracked microenvironmental forces over time during ASC self-assembly into spheroids as well as during uptake into pre-formed spheroids. Additional experiments investigated measurement fidelity for selected MP elasticities and the effect of cytoskeletal inhibitors on cellular forces in a 3D environment.

2. Methods

2.1. HCMP fabrication, coating, and characterization

Hyper-compliant microparticles (HCMPs) were fabricated using an inverse emulsion polymerization protocol [15]. Briefly, HCMPs were created using a 4% acrylamide to 0.05% bis-acrylamide solution (Bio-Rad). HCMPs were serially filtered through 100, 70, and 40 μm mesh filters to decrease size dispersity. A triphenylmethane dye (Sharpie) with an excitation at 640 nm and emission at 670 nm was added for visualization. MPs produced using a microfluidic flow-focusing droplet generator produce 33 μm in diameter (Fig. S1) using 3.9% acrylamide to 0.22% bis-acrylamide solution in 5 mg of ammonium persulfate (APS, MilliporeSigma), 2.5 mg of lithium phenyl-2,4,6-trimethylbenzoylphosphinate (LAP, $\geq 95\%$, MilliporeSigma), 50 μL of fluorescent dye, and de-ionized (DI) water [20]. A subset of HCMPs and MPs had sulfo-SANPAH (#13414, CovaChem) UV-photoactivated onto their surface followed by covalent binding of 100 mg/mL collagen type 1 (COL-1, #08–115, Lot #2373345, Millipore) via overnight incubation at 4 °C. Non-coated HCMPs were used as controls. HCMPs were mechanically characterized using an MFP-3D-Bio atomic force microscope (AFM, Asylum Research) following previously established techniques [21]. In brief, individual HCMPs and MPs were indented using a cantilever with a spherical tip while recording the force applied and indentation into the material ($n = 20$, $n = 9$). From these data, the elastic modulus (E) was calculated using the Hertz model for spherical indentation.

2.2. Cell culture

Human adipose-derived stem cell superlot #36 (comprised of 5 female donors) (Zen-Bio, Inc.) passage 4 to 6 were cultured in medium consisting of DMEM/F-12, 1% antibiotic/antimycotic (Hyclone), 10% FBS (Zen-Bio, Inc.), 1 ng/mL fibroblast growth factor, 5 ng/mL epidermal growth factor, and 0.25 ng/mL transforming growth factor- β 1 (R&D Systems) and expanded at 37 °C in 5% CO₂. Once 80–90% confluent, cell monolayers were washed once with DMEM/F-12 and uplifted using 0.05% trypsin and incubated for 5 min at 37 °C in 5% CO₂. Trypsin was neutralized using culture medium and cell were then concentrated by centrifugation at 400g for 5 min. Cells were resuspended in culture medium and counted prior to experimentation [16,22,23].

2.3. 3D spheroid assembly and image acquisition

To encourage spheroid formation, ASCs were seeded into hydrogel microtissue arrays [22,23]. To create the arrays, 100 μL of sterile, 2% molten agarose (Fisher Scientific) solution was added to each well of a 96-well plate (Greiner bio-one, #655891) and stamped with a mold to form four, conical-shaped microwells (Microtissues, Inc). Hydrogels solidified for 15 min at room temperature before the mold was removed, followed by overnight equilibration in 150 μL of DMEM/F-12 with 1% Penicillin-Streptomycin at 37 °C in 5% CO₂ prior to experimentation. A 20 μL aliquot of ASC suspension was pipetted into the loading dock of each hydrogel to form four spheroids each composed of about 1500 cells in conjunction with ~ 1 –2 HCMPs. To accelerate spheroid formation and subsequent mesenchymal condensation, seeded plates were centrifuged for 2 min at 200 g. Following centrifugation, each well was gently flooded with 150 μL of growth medium.

Two different assays were included to examine cell-HCMP interaction and force generation. The first assay investigated uptake of collagen-coated and non-coated HCMPs into 7-day, pre-formed spheroids (Fig. 1a). This experiment determined whether cells could directly interact with the force sensors, while also providing a means to examine forces in the shell and core regions of the spheroid for HCMPs that were taken up. The second assay investigated forces present during a model mesenchymal condensation process. Both collagen-coated and non-coated HCMPs were incorporated into spheroids as the cells self-assembled into compact structures.

Spheroids were imaged using an Opera Phenix™ High Content Screening System (PerkinElmer). An inverted 5X air objective lens along with a bright-field microscopy prescan protocol was used to locate all four conical-shaped microwells containing cells. Upon locating microwells, a 20X water objective with a Cy5 filter set (640ex/670em), 100 ms exposure time, and 50% excitation power were used to visualize red dye-stained HCMPs. Z-slices were separated by 2 μm for a total imaging depth of 200 μm , captured repeatedly at 1-h time intervals for up to 14 h.

2.4. Cytoskeletal inhibitors and live/dead viability assay

Cytoskeletal inhibitors were prepared in DMSO as stock solutions as follows: Cytochalasin D (C8273, Sigma, 1970 μM), and Y27632 (catalogue no. HY-10583, Medchemexpress, 100 μM). Immediately prior to use, stocks were diluted with culture medium to a final concentration of 2 μM CytoD and 10 μM Y27632. Spheroids containing HCMPs were self-assembled and allowed to condense over 12 h. These samples were then treated with inhibitors for 12 h, after which they were washed three times with culture medium and allowed to recover for 6 h. The morphology, viability, and force profiles of these samples before, during, and after treatment were compared to control samples exposed to either culture medium containing DMSO or culture medium only.

A live/dead viability/cytotoxicity kit (catalogue no. L3324, ThermoFisher Scientific) was used to determine whether the cytoskeletal inhibitors affected spheroid viability. In brief, calcein AM (live cells, 1:2000 dilution) and ethidium homodimer-1 (dead cells, 1:500 dilution) were mixed in culture medium, added to wells containing spheroids, and incubated for 45 min at 37 °C in 5% CO₂. After incubation, wells were washed gently twice and re-filled with fresh culture medium. Spheroids were immediately imaged at 488ex/515em for calcein AM and 561ex/617em for ethidium homodimer-1.

2.5. Image processing and data analysis

Time-lapse, confocal z-slice images of HCMPs were collected from their original, non-deformed state at time 0 through all deformed states. ImageJ (NIH) was used to focus on HCMPs and set image intensity to be the same across all images and converted to 8-bit prior to running all images through Wolfram Mathematica®.

We developed an integrated 3D cell traction estimation computer

program using the Wolfram Language™. The stress calculations module of the program takes the confocal z-stack images of a HCMP from two time instances as input. At the earlier of the two time instances, the HCMP needs to be outside the ASC spheroid. The module returns the HCMP's stress field at the later of the two time instances as output. A post-processing module takes the stress field as input and can generate representations such as contour plots of various stress components (Fig. 1d) and vector plots of HCMP traction fields (Fig. 1e and f). It can also integrate the stress field over the HCMP volume to calculate average

internal pressure and stored elastic energy density, which is representative of the absolute deformation of a force sensor by the surrounding microenvironment. These two metrics complement each other, since the average pressure provides insight into the nature of the overall deformation, i.e., whether the HCMP is contracting or expanding, while the elastic energy density provides insight into the intensity of the overall deformation, i.e., a large elastic energy density implies that the HCMP is greatly deformed from its baseline shape.

On being provided with a family of z-stacks each of which

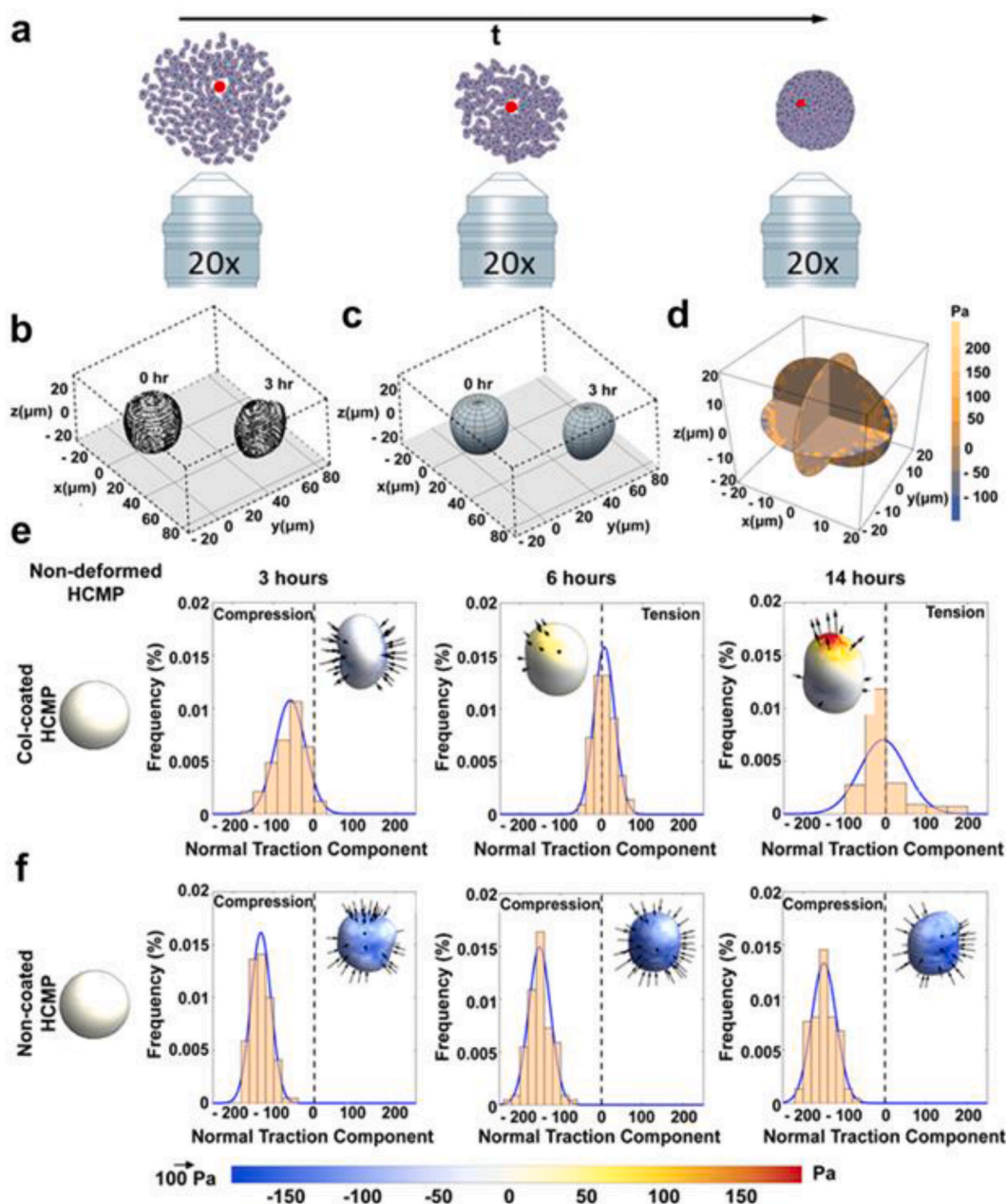


Fig. 1. Illustration of HCMP processing steps for quantifying microenvironmental forces. (a) Cells (purple) and HCMPs (red) at initial seeding through spheroid formation and compaction. (b) Image processing algorithms identified the surface of HCMPs as point clouds. (c) Spherical harmonic basis functions were fit to point clouds in (b) to construct smooth, analytical representations of the HCMP surfaces. The shape of the un-deformed HCMP was used as the reference (stress-free) state for the finite element-based stress calculations. (d) Contours of the stress component σ_{12} are shown on the HCMP's undeformed configuration for a representative case. (e) HCMP surface traction information at three time instances during mesenchymal condensation is shown for a representative, collagen-coated HCMP, which experienced both compressive and tensile forces (denoted by arrows) on its surface. (f) Similarly, traction data at the same time points are shown for a representative, non-coated HCMP, which experienced solely compressive forces. In (e) and (f), the colors in the insets correlate with the values of the HCMP surface's normal traction component, with negative values (compressive traction vectors) corresponding to blue colors and positive values (tensile traction vectors) to yellow/red colors. The arrows in the insets denote the surface traction vectors. Traction vectors with a magnitude smaller than a tolerance value of 50 Pa are not shown. (For interpretation of the references to color in this figure legend, the reader is referred to the Web version of this article.)

corresponds to a different time instance the program runs the stress-calculation module iteratively to generate the time series of the HCMP's average internal pressure and elastic energy density. These plots can provide insight into how those quantities evolve over time.

The stress-calculation module is mainly composed of the image-processing and the finite element analysis (FEA) submodules.

The image processing submodule takes a z-stack of confocal microscopy images as input. It is not necessary that at the time instance corresponding to that z-stack the HCMP be outside the ASC spheroid. The HCMP's surface points are identified in each image of the z-stack using edge detection algorithms. The surface points from all images from the z-stack are combined to generate a 3D point cloud (Fig. 1b) representation of the HCMP's surface. This discrete representation of the HCMP's surface can be used to compute quantities related to the HCMP's geometry, such as volume, average radius, surface area etc., however, we could not use it directly for computing quantities related to the HCMP's mechanics, such as pressure, elastic energy density, etc. Spherical harmonic basis functions are fit to the 3D point cloud to generate a smooth, analytical representation of the HCMP's surface. We were able to compute the HCMP's mechanics quantities of interest using this smooth representation.

The FEA sub-module takes the smooth, analytical representation of the HCMP's surface from two different time instances as input. As we mentioned earlier, the HCMP is required to be outside the ASC spheroid at the earlier of the two time instances. We denote the analytical surfaces from the two time instances as Γ_0 and Γ_t , respectively, with Γ_0 corresponding to the earlier of the two time instances. Analogously, we denote the HCMP's configurations in the two time instances as \mathcal{B}_0 and \mathcal{B}_t , respectively (e.g., see Fig. 1c). We assume that \mathcal{B}_0 is a stress-free state. Say a material particle \mathcal{X} has the position vectors $X(\mathcal{X})$ and $x(\mathcal{X})$ in \mathcal{B}_0 and \mathcal{B}_t , respectively, then we call the quantity $x(\mathcal{X}) - X(\mathcal{X})$ the material particle \mathcal{X} 's displacement at the time instance t . Identifying a material particle with its position vector in \mathcal{B}_0 , we can alternately state that the displacement of the material particle X (i.e., the material particle \mathcal{X} that in the reference configuration \mathcal{B}_0 has the position vector X) is $x(X) - X = : u_t(X)$, where $x(X)$ is X 's (or to be more precise \mathcal{X} 's) position vector in \mathcal{B}_t . The function $u_t : \mathcal{B}_0 \rightarrow \mathcal{B}_t$ is called the HCMP's displacement field.

The HCMP is composed of polyacrylamide [24]. We assume that the PA mechanical properties are spatially uniform over the HCMP and do not change as the HCMP interacts with the ASC spheroid.

We model the PA material's mechanics using the linear theory of elasticity. We start by assuming that the PA's mechanical stress-strain behavior is dictated by the Saint Venant–Kirchhoff constitutive law. As per this law, the 2nd Piola–Kirchhoff stress tensor at a material particle X , $S(X)$, is related to the Green–Lagrange strain tensor at that point $E(X)$ as

$$S(X) = 2\mu E(X) + \lambda I \text{tr}(E(X)), \quad (1)$$

where I is the identity tensor, $\text{tr}(\cdot)$ is the trace operator, and λ and μ are Lamé's parameters. We use values of 705.56 Pa and 90.78 Pa, respectively, for these parameters. These values are based on Atomic Force Microscopy enabled contact mechanical testing of our HCMP particles, which we carried out previously [21]. The tensor $E(X)$ is defined as

$$E(X) = \frac{1}{2} (F^T(X)F(X) - I), \quad (2)$$

where $F(X) = I + u_t'(X)$, and u_t' is the Fréchet derivative of u_t . We obtain the displacement field u_t by solving the static form of the Cauchy-momentum equation, which is

$$\text{Div}(F(X)S(X)) = \mathbf{0}, \quad \forall X \in \mathcal{B}_0. \quad (3)$$

By postulating that the HCMP's displacement field u_t satisfies (3) we are implicitly assuming that the loading on the HCMP by the ASCs is quasi-static in nature.

To solve (3) it is necessary to prescribe boundary conditions on u_t . Due to the featureless nature of the HCMP's surface it was not possible for us to experimentally determine the position vectors of the HCMP's surface material particles in the deformed configuration \mathcal{B}_t . Consequently, we do not know the value of u_t on Γ_0 from our experiments. Owing to the spherical geometry of the HCMP in the reference configuration, we posit that, as an alternative, it is reasonable to assume that

$$x(X) = \text{argmin}\{\|y - X\| : y \in \Gamma_t\}, \quad \forall X \in \Gamma_0, \quad (4)$$

and construct the boundary condition for u_t simply as

$$u_t(X) = x(X) - X, \quad \forall X \in \Gamma_0, \quad (5)$$

where the values of $x(\cdot)$ in (5) are given by (4).

As mentioned previously, we use the linear theory of elasticity for modeling the mechanics of the HCMP. In line with that theory, for the remainder of the analysis we set $F(X)$ to be equal to I in (3) and set $E(X)$ equal to the small strain tensor $(u_t'(X) + u_t'^T(X))/2$ in (1). Following these approximations, we solve equations (1)–(5) for u_t numerically using linear, finite element techniques [25].

Using the solution u_t and computing S from (1) we calculate the traction vector at the surface point X , which we denote as $T(X)$, from its definition, which is that $T(X) = F(X)S(X)\hat{N}(X)$. Here \hat{N} is the outward unit normal to Γ_0 at X . We similarly compute the normal component of the traction vector as $T(X) \cdot \hat{N}$. We compute the stored elastic energy density of the HCMP as

$$\hat{\Pi} = \frac{1}{\text{vol}(\mathcal{B}_0)} \int_{\mathcal{B}_0} \left(\frac{\lambda}{2} (\text{tr}(E(X)))^2 + \mu \text{tr}(E(X)E(X)) \right) d\Omega_0, \quad (6)$$

where $\text{vol}(\mathcal{B}_0)$ is the volume of \mathcal{B}_0 .

The value of the pressure field at the position vector x in \mathcal{B}_t is

$$p(x) = \frac{1}{3} \text{tr}(\sigma(x)), \quad (7)$$

where

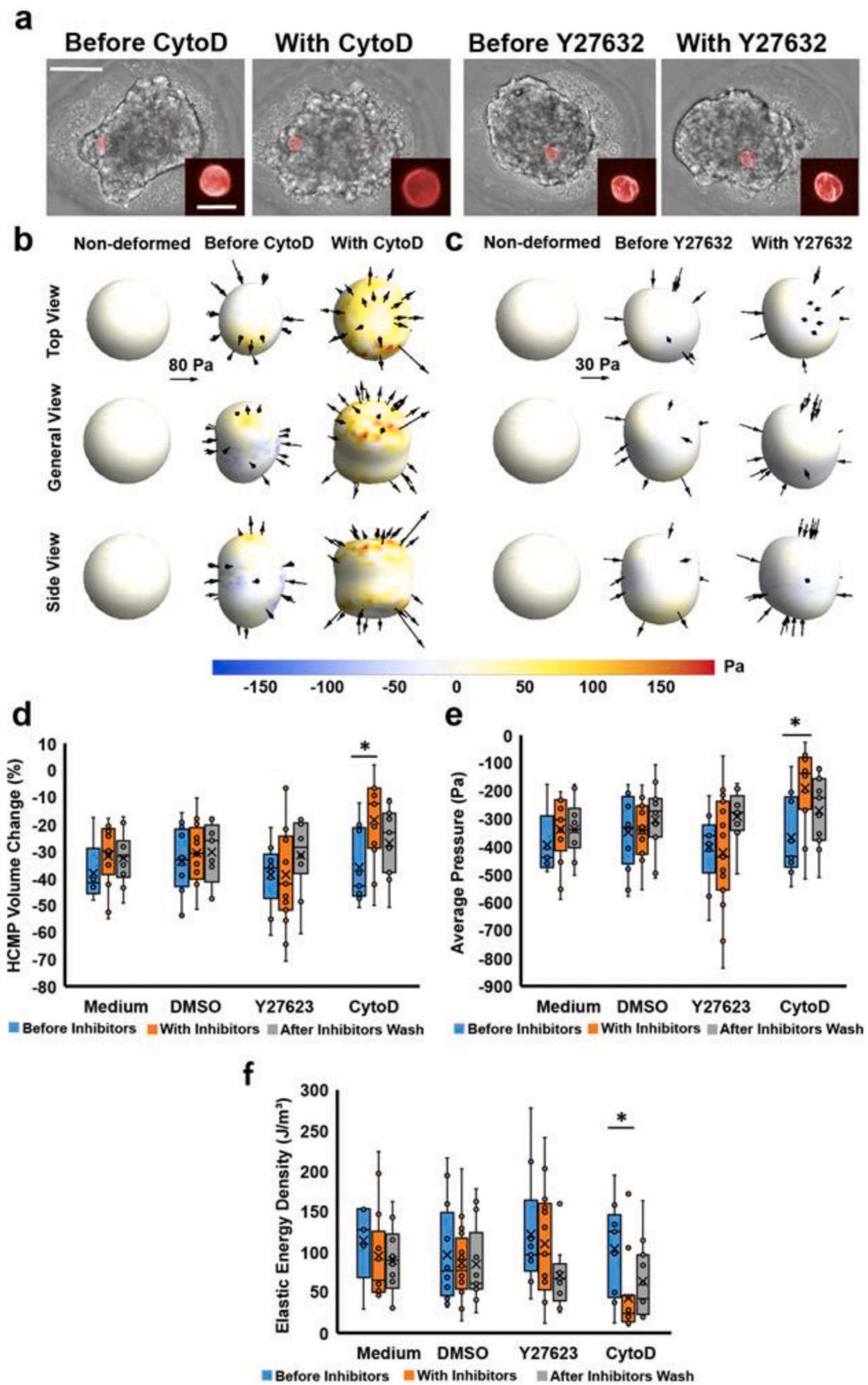
$$\sigma(x(X)) := \frac{1}{\text{Det}(F(X))} F(X)S(X)F^T(X), \quad (8)$$

and $\text{Det}(\cdot)$ is the determinant operator. In solid mechanics literature, it is more common to define pressure as the negative of the quantity on the right-hand side of (7). However, we use (7) to define pressure, since we believe that the pressure defined this way is more intuitive in the present context. Keeping in line with the linear theory of elasticity we set $F(X)$ and $F^T(X)$ to be equal to I in (8) and compute the average pressure in the HCMP as

$$\langle p \rangle = \frac{\int_{\mathcal{B}_0} p(x(X)) \text{Det}(F(X)) d\Omega_0}{\int_{\mathcal{B}_0} \text{Det}(F(X)) d\Omega_0}. \quad (9)$$

2.6. Statistical analysis

All statistical analyses were performed using SigmaPlot 12.5 (Systat Software, Inc). T-tests were used to compare the uptake rate of collagen-coated and non-coated HCMPs. Dixon's Q tests were used with a t -test to differentiate pressure and elastic energy density data for the position of



(caption on next page)

Fig. 2. Cytoskeletal inhibitor effects on cell/spheroid morphology and microenvironmental forces. (a) Changes in HCMP (red, scale bar: 25 μm) and spheroid (scale bar: 100 μm) morphology after treatment with the chemical inhibitors cytochalasin D (CytoD) or Y27632 ($n = 8$ for culture medium, $n = 13$ for DMSO, $n = 11$ for CytoD, $n = 10$ for Y27632). Spheroids treated with CytoD exhibited clear morphological changes, with HCMPs tending to revert to a less-deformed shape. Representative depiction of an HCMP showing total traction forces before and after (b) CytoD and (c) Y27632 treatment. More extensive size changes and traction force characteristics were observed for CytoD samples than Y27632. (d) HCMP volume, (e) average pressure, and (f) elastic energy density measurements made before, during, and after exposure to Medium, DMSO, Y27632, and CytoD. Each circle shown corresponds to a single HCMP measurement for a distinct spheroid. Solid lines in the box plots correspond to the minimum, 25th percentile, median, 75th percentile, and the maximum, while the x coincides with the mean. No statistically significant differences were found except when spheroids were treated with CytoD (before vs. with inhibitors, $*P < 0.05$). (For interpretation of the references to color in this figure legend, the reader is referred to the Web version of this article.)

collagen-coated HCMPs within spheroids. T-tests were performed to assess differences in percent change of volume, pressure, and elastic energy density of HCMPs before and after inhibitors. For all statistical analyses, significance was achieved at $p < 0.05$.

3. Results

3.1. HCMP coating influences the type and directionality of cell-particle interactions

Experiments involved seeding ~ 6000 ASCs into non-adhesive, agarose microwell arrays and allowing the cells to undergo mesenchymal condensation into spheroidal microtissues (Fig. 1a). ASC spheroids formed within hours and compacted into cohesive microtissues in less than half a day. Next, experiments used HCMPs to track the microenvironmental forces of self-assembling ASCs over 10–14 h after initial seeding. To record HCMP deformation, spheroids were imaged in 3D using an Opera Phenix High-Content Imaging System. Z-stack images captured HCMPs in their initial, non-deformed shape and at hourly time points, reflecting changes that occurred in response to forces within the neotissues. For each selected time, a Z-stack of images were first processed to construct a 3D point cloud (Fig. 1b). Then, spherical harmonic basis functions were used to create smooth analytical representations of the HCMP surface (Fig. 1c). Using the linear theory of elasticity, we determined the HCMP stress field using finite element analysis. Contours of the stress component σ_{12} from a representative finite element calculation are shown on the HCMP reference configuration (Fig. 1d). From the stress field, the traction vectors on the HCMP surface were recorded with only the large normal traction component vectors showing (Fig. 1e–f). As a simple net measure of all the forces acting on the HCMP, the average pressures in the HCMP was calculated. We define pressure at a point as one third the trace of the stress tensor. Additionally, we calculated the elastic energy density of the HCMP, defined as the volume average of the total elastic energy stored within the HCMP. This metric was indicative of the absolute deformation of the HCMP and independent of the compressive/tensile nature of the external forces. Fig. 1e displays the deformed configuration of a collagen-coated HCMP and the tractions experienced over time as ASCs underwent condensation and self-assembly (tensile and compressive forces). Comparatively, non-coated HCMPs experienced predominantly compressive (pushing) forces since cells could not directly bind and pull on them providing a tensile force (Fig. 1f).

3.2. Microtissue uptake of HCMPs facilitated by collagen type I coating

Experiments investigating the interaction of pre-formed, 7-day spheroids with newly added HCMPs showed that collagen-coated HCMPs were taken up by the microtissue, indicating a direct cell-HCMP interaction, while non-coated HCMPs remained excluded, showing a lack of direct interaction (Fig. S2). The directionality of forces across the surface of HCMPs also differed between the shell and core regions of the spheroid. HCMPs in the shell exhibited shapes elongated in the circumferential direction, suggesting more tensile forces along the major axis. HCMPs near the core exhibited rounded shapes, suggesting more uniform compressive forces (Fig. S2c, d). Force measurements for HCMPs at the core of the spheroids showed that pressure was more

variable than HCMPs at the periphery/shell (Fig. S2e), whereas elastic energy density was similar across the two regions (Fig. S2f).

3.3. HCMP measurements reflect changes in cell forces and morphology due to cytoskeletal inhibitors

The cytoskeletal inhibitors cytochalasin D (CytoD) and Y27632 were used to inhibit actin polymerization and cellular contractility, respectively, to verify that HCMP deformation corresponded to cellular force generation (Fig. 2). CytoD treatment displayed morphological changes in the spheroids, with cells becoming more rounded and the spheroid appearing less cohesive (Fig. 2a & b). Using HCMP volume measurements as a simple proxy for mechanical changes, CytoD exposure resulted in $\sim 15\%$ increase in volume (Fig. 2d). A corresponding loss of calculated, compressive forces could be observed using the force sensors (Fig. 2e). When CytoD was removed from the samples, HCMP volume decreased $\sim 10\%$, with a corresponding increase in compressive forces, which approached the values measured before CytoD treatment. Elastic energy density showed a similar trend (Fig. 2f). These results are hypothesized to occur due to the inability of cells to generate forces when treated with CytoD, producing an overall lessening of the compressive environment within spheroids. In some cases, average pressures on HCMPs have been observed to be tensile, which can occur when multiple, opposing cell adhesions on an HCMP surface are pulled by surrounding cells that are rounding up. Y27632 treatment had no discernible effect on cell/spheroid morphology (Fig. 2c), a finding similar to previously published work [9]. Measurements showed no statistically significant change in HCMP volume, average pressure, or elastic energy density. However, a slight increase in average pressure and decrease in elastic energy density was noted after removal of Y27632, potentially indicating the resumption of cell-HCMP tensile forces upon restoration of Rho/ROCK activity. Cell viability before, during, and after exposure to cytoskeletal inhibitors was unchanged across all exposure groups (Fig. S3).

3.4. Microenvironmental forces stabilize over time during mesenchymal condensation

Next, a model condensation assay was used in which ASCs and HCMPs were seeded simultaneously into agarose microwells and monitored during self-assembly. Both non-coated and collagen-coated HCMPs were found to integrate into the microtissue, being gathered up as the cells coalesced into a compact spheroid. HCMP deformation resulted from the direct (collagen-coated HCMPs) and indirect (non-coated and collagen-coated HCMPs) interactions with surrounding cells. For this assay, HCMPs tended to be positioned in the core region of the spheroid, rather than the shell, as a consequence of cell movement during condensation. ASCs self-assembled within approximately 5 h, with only minor morphological changes to the spheroid over the remaining time (Fig. 3a). Forces varied widely during the initial stages of condensation but settled as spheroids became more cohesive. This pattern was observed for both collagen-coated and non-coated HCMPs (Fig. 3b–e). Initially, compressive forces were dominant across HCMP surfaces. However, at later time points, less consistent directionality was observed to the forces. Average pressure for collagen-coated HCMPs at their steady-states ranged from -600 to 100 Pa, with most spheroids

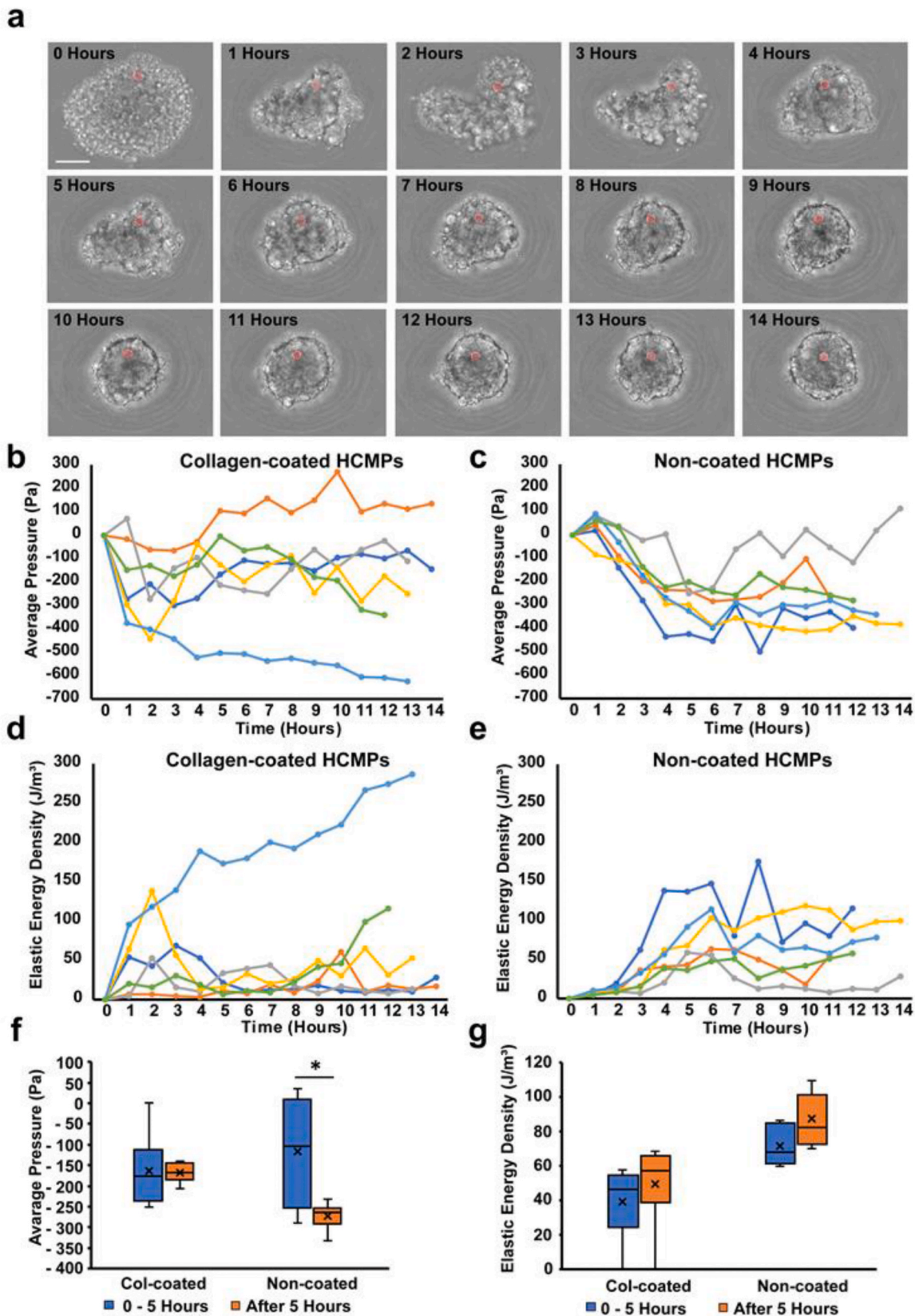


Fig. 3. Microenvironmental forces present during early mesenchymal condensation. (a) Brightfield image displaying cellular self-assembly with embedded HCMP (red) over a period of 14 h. As condensation proceeded, HCMPs were predominantly positioned in the core region. Average pressure measured using (b) collagen-coated and (c) non-coated HCMPs. Elastic energy density measured using (d) collagen-coated and (e) non-coated HCMPs. (f) Sample average pressure and (g) elastic energy density for the first 5 h (early condensation) compared to the remaining time points (later condensation), depicted for both collagen-coated and non-coated HCMPs. * $P < 0.05$. Scale bar: 100 μm . (For interpretation of the references to color in this figure legend, the reader is referred to the Web version of this article.)

settling at approximately -150 Pa. Comparatively, non-coated HCMPs ranged between -400 and -100 Pa, with most spheroids settling at approximately -250 Pa. Pressures exerted in the latter case can be attributed to indirect interactions with surrounding cells, providing a general measure of the internal pressurization of the spheroids (Fig. 3f). Positive and negative values reflect tensile and compressive forces, respectively. Compressive forces were hypothesized to be driven by the communal network of cells in the microtissue, creating hydrostatic pressurization as they pulled on each other and compacted the larger structure. Elastic energy density values tended to mirror the average pressure, with a stabilization occurring after 5 h once the condensation process transitioned cells to a more cohesive organization (Fig. 3c & e). Also, for most spheroids evaluated in this study, the elastic energy density within HCMPs was small, averaging under 120 J/m³ (Fig. 3g). This suggests that the overall shape changes experienced by HCMPs were not dramatic in either tensile or compressive directions relative to the reference state, emphasizing the need for highly sensitive force sensors that can detect small stresses exerted within biological systems.

3.5. HCMP elastic modulus influences measurement sensitivity and precision

To investigate the importance of MP stiffness on measurement fidelity, we conducted experiments comparing the forces exerted on our HCMPs to those measured for MPs of the same size and material but with a higher elastic modulus (1.77 ± 0.04 kPa), roughly equivalent in magnitude to MPs used in recent works [9,10,12]. Fig. 4a and b shows representative deformations experienced by both MP types during the condensation process. Deformation was 1.5–2.5 times greater for HCMPs than the stiffer MPs when comparing changes in force sensor volume (Fig. 4c). That said, the average pressure measured using either MP type was approximately the same (Fig. 4d). The major difference was in the range of values reported, with the stiffer MPs reflecting substantially more variability in their measurements than the HCMPs (-1.5 – 0.5 kPa vs. -0.5 – 0 kPa, respectively). Elastic energy density measurements showed similar variability characteristics for the two MP types, with overall higher average values for the stiffer variety (Fig. 4e). The large range of values for stiffer MPs reflect the uncertainty associated with

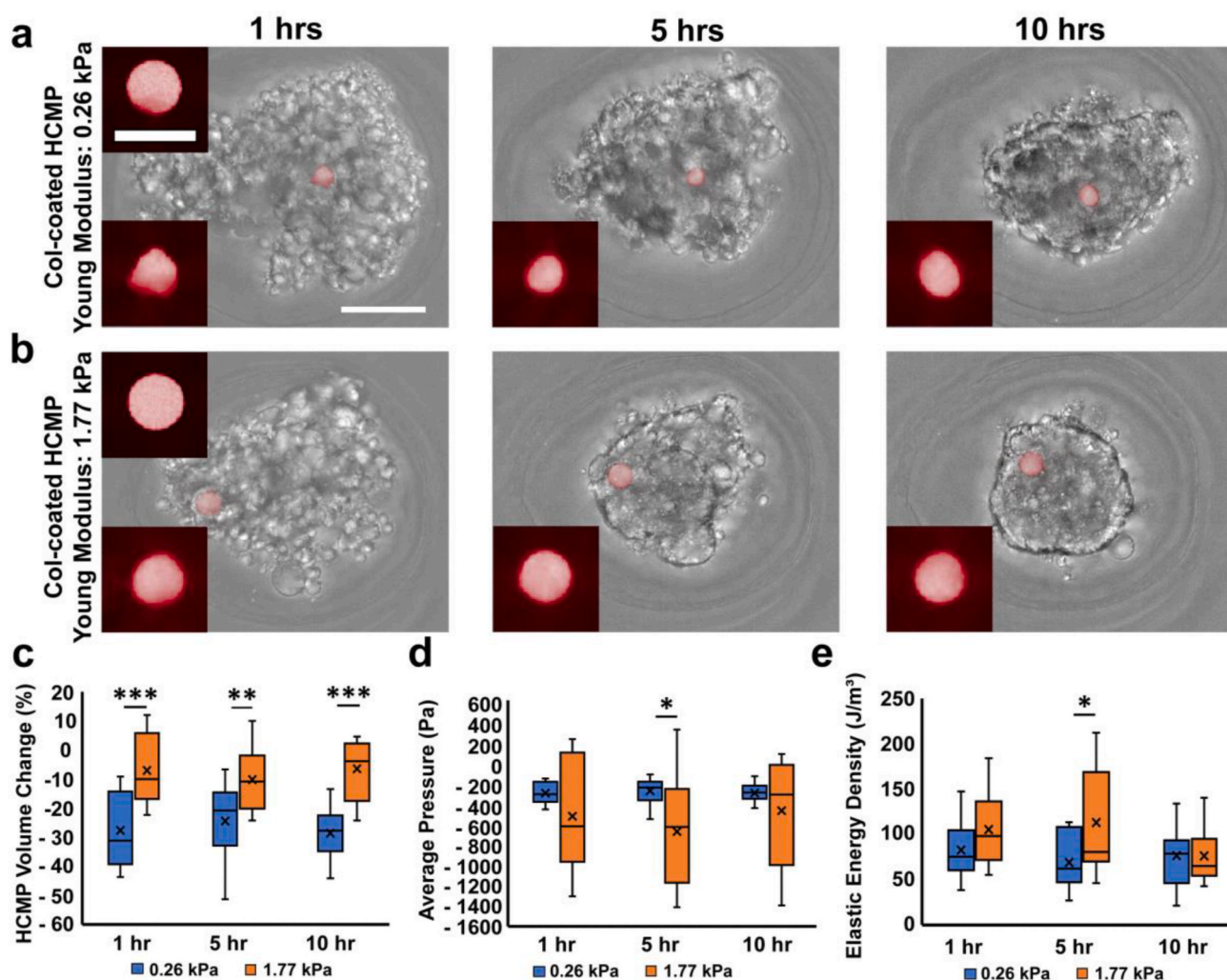


Fig. 4. HCMP modulus influences measurement sensitivity. (a) Highly compliant, Col-coated HCMPs (red coloring, 0.26 kPa, scale bar: 50 μ m) exhibited large deformations within spheroids at all-time points (scale bar: 100 μ m). Non-deformed HCMP shown in top left inset. (b) Less compliant, Col-coated initial HCMPs (1.77 kPa) deformed to a noticeably lesser extent. Graphs show (c) change in HCMP volume, (d) average pressure, and (e) elastic energy density (0.26 kPa, $n = 13$; 1.77 kPa, $n = 10$). Solid lines in the box plots correspond to the minimum, 25th percentile, median, 75th percentile, and the maximum, while the x coincides with the mean. Student's t-test determined significant differences, *** $P < 0.001$, ** $P < 0.01$, and * $P < 0.05$. Comparisons between the two HCMP types showed slight differences in mean values, with the highly compliant varieties having substantially lower errors associated with their measurements. (For interpretation of the references to color in this figure legend, the reader is referred to the Web version of this article.)

imaging small deformations within a living, biological system that contains substantial noise. As such, HCMPs were found to have not only greater sensitivity by also greater precision than the stiffer MP formulation.

4. Discussion

Mechanical cues play an important role in tissue assembly and morphogenesis, contributing to fate determination in many tissues [10, 12]. While tools exist for directly measuring forces at macro- and molecular-scales, it has been more challenging to do so at microscales, especially in cell dense biological systems. Here, we demonstrated how non-disrupted, biocompatible, mechanically defined, highly-sensitive HCMPs can be used to repeatedly and non-destructively quantify the pressure and elastic energy density of cellular microenvironments during mesenchymal condensation. The mathematical models used to calculate the forces in 3D exerted on HCMPs revealed the presence of anisotropic pressure during the initial formation of microtissues. Hydrostatic pressurization was achieved at later time points due to the collective work of cells as they came together and formed tight junctions and compaction of the neotissue.

HCMPs reflected the mechanical forces experienced by cells in part due to their cell-like characteristics, including protein-ligand binding, size, and deformability. Notably, the exertion of tensile forces on them were found to be dependent on the presence of a surface coating. Collagen type I allowed for cell-HCMP adhesions to form which could then be pulled on by the surrounding cells, a behavior that has been noted previously for MPs coated with RGD (Arg-Gly-Asp) peptide [10]. Comparatively, application of compressive forces appeared to be independent of HCMP coating or non-coating. Deformed HCMP shapes varied widely within microtissues; however, they tended to mimic the morphology of neighboring cells by region. This included having an elongated shape at the periphery and a rounded shape at the core, morphologies common to fibroblast-like cells in spheroid model systems [10,12,26]. Cell shape influences the type and magnitude of forces that can be exerted, and thus, plays an important role in contributing to cell-generated pressures present during tissue organization and growth [8,27,28].

The variability in measured microenvironmental forces in the current study was substantial, particularly when compared across multiple, independent spheroid samples. This was to be expected considering the numerous arrangements for how a collection of cells can bind to each other and exert forces on intervening HCMPs during the self-assembly process. However, we were able to narrow the range of measured values by using more sensitive MP sensors, i.e., hyper-compliant varieties, whose deformations were large enough to be reliably imaged in a noisy, 3D culture environment. Additional refinements to the

HCMPs themselves, including improved fluorescent signal and monodispersity, are likely to further reduce experimental variability [20]. Regardless, large sample sizes will be critical for future investigations that seek to parse out fine differences. Here, we demonstrated that these types of experiments could be conducted in a parallelized fashion using a high-content imaging system containing up to 384 microwells. While the computational component still requires significant time, a large number of experimental conditions can be included and explored at once using this approach. These refinements will allow researchers to better explore how microenvironmental forces influence tissue assembly.

While we observed a consistent transition between a seemingly random, early force profile to a more steady-state one, the biological relevance of that mechanical state is not currently clear. Changes in cell-cell adhesions and mechano-related intracellular signaling molecules are likely occurring throughout this process and will contribute to the larger, microenvironmental forces measured by the HCMPs. While the current study was not designed to delve into specific, mechanobiological queries, the testing platform should be well-suited to do so, particularly

since it is compatible with a highly arrayed setup that can simultaneously assess hundreds of samples. This will be needed to account for the substantial variability observed from spheroid-to-spheroid and HCMP location within spheroids. Previous work has observed a similar lessening of morphological changes in spheroids when they begin compacting [29]. As it currently stands, the early fluctuation of forces we observed is hypothesized to be driven by heterogeneity in the ASC population, self-assembling into microtissues at different rates and shape uniformity. As cells condensed into geometrically similar structures, overall forces became more consistent for any given force sensor. The “steady-state” average pressures of -150 Pa for collagen-coated HCMPs and -250 Pa for non-coated HCMPs measured for ASC spheroids provide some insight on cellular contributions to these forces. Namely, the ability to directly interact with the force sensors can partially offset the large, compressive forces that uniformly occur during condensation. Because of the localized nature of the HCMPs, it is important to note that force profiles appeared to be influenced by their final location within spheroids (e.g., shell vs. core) so were not necessarily representative of the entire biological unit. Spatial force mapping of a full microtissue with HCMPs is certainly possible, although force sensor positioning in the structure would be largely up to random chance. More HCMPs could be included in each microtissue to help with this, but a better alternative would be to simply increase the number of samples using a highly arrayed setup to minimize the potential for cell-HCMP interactions to influence the overall biological behavior of the sample. The current study used $\sim 1-2$ HCMPs within hundreds/thousands of ASCs to limit any potential effects of this sort. While tensile forces were observed for measurements in both the core and shell regions of the spheroids, compressive forces were much larger and more prevalent. This likely reflects the mechanical consequences of tight junction formation among cells as they self-assemble and condense into cohesive biological structures. These observations emphasize the need to consider spatial information along with quantitative measurements in the future, i.e., via microenvironmental force maps through aggregated data.

5. Conclusions

Mechanical cues play an integral role in developmental processes. The data shown here quantify for the first time the forces present as ASCs self-assemble and organize into a spheroid, modeling the mesenchymal condensation process. The presented technique introduces real-time tracking of force measurements in an arrayed, 3D system using novel HCMPs as force sensors to measure local traction forces applied by cells within microtissues, with sensitivity down to tens of Pascals. The advances in force sensor sensitivity and demonstrated ability to collect spatiotemporal information open the doors for studying dynamic biological events driven by local cells. Beyond fundamental investigations of forces in development and morphogenesis, our method can potentially serve in any number of situations that seek microscale mechanical measurements with minimal disruption of the larger tissue structure, which could include studies of tissue repair and remodeling, tumor microenvironments, or organoid model systems. Lastly, the highly arrayed testing platform described herein allows for the possibility of microenvironmental force-based screening of cell spheroids containing HCMP sensors following exposure to drugs, toxins, or other chemicals.

Authors' contributions

Robert Gutierrez: Methodology, Validation, Formal analysis, Investigation, Writing – original draft, Visualization Wenqiang Fang: Methodology, Software, Data curation, Writing – review & editing, Visualization Haneesh Kesari: Methodology, Software, Data curation, Resources, Writing – review & editing, Supervision, Funding acquisition Eric M. Darling: Conceptualization, Resources, Writing – review & editing, Supervision, Project administration, Funding acquisition

Data availability

All data needed to evaluate the conclusions in the paper are already included and/or available within the Supplementary Materials. Additional data related to this paper may be requested from the authors.

Image processing and data analysis code available at: https://github.com/wqfang/HCMP_Project.

Declaration of competing interest

The authors declare that they have no known competing financial interests or personal relationships that could have appeared to influence the work reported in this paper.

Acknowledgements

This research was supported by Brown University's Center to Advance Predictive Biology, National Institutes of Health (NIH) (R01 AR063642 to EMD), Brown University Seed Award (HK, EMD), and National Science Foundation GRFP (2018260690 to RAG).

Appendix A. Supplementary data

Supplementary data to this article can be found online at <https://doi.org/10.1016/j.biomaterials.2021.120684>.

References

- [1] T. Lecuit, P.-F. Lenne, Cell surface mechanics and the control of cell shape, tissue patterns and morphogenesis, *Nat. Rev. Mol. Cell Biol.* 8 (8) (2007) 633.
- [2] T. Mammoto, D.E. Ingber, Mechanical control of tissue and organ development, *Development* 137 (9) (2010) 1407–1420.
- [3] M.A. Schwartz, Integrins and extracellular matrix in mechanotransduction, *Cold Spring Harbor perspectives in biology* 2 (12) (2010), a005066.
- [4] M. Dembo, T. Oliver, A. Ishihara, K. Jacobson, Imaging the traction stresses exerted by locomoting cells with the elastic substratum method, *Biophys. J.* 70 (4) (1996) 2008–2022.
- [5] W.R. Legant, J.S. Miller, B.L. Blakely, D.M. Cohen, G.M. Genin, C.S. Chen, Measurement of mechanical tractions exerted by cells in three-dimensional matrices, *Nat. Methods* 7 (12) (2010) 969.
- [6] J.L. Tan, J. Tien, D.M. Pirone, D.S. Gray, K. Bhadriraju, C.S. Chen, Cells lying on a bed of microneedles: an approach to isolate mechanical force, *Proc. Natl. Acad. Sci. Unit. States Am.* 100 (4) (2003) 1484–1489.
- [7] E. Cukierman, R. Pankov, D.R. Stevens, K.M. Yamada, Taking cell-matrix adhesions to the third dimension, *Science* 294 (5547) (2001) 1708–1712.
- [8] O. Campàs, T. Mammoto, S. Hasso, R.A. Sperling, D. O'connell, A.G. Bischof, R. Maas, D.A. Weitz, L. Mahadevan, D.E. Ingber, Quantifying cell-generated mechanical forces within living embryonic tissues, *Nat. Methods* 11 (2) (2014) 183.
- [9] M. Dolega, M. Delarue, F. Ingremeau, J. Prost, A. Delon, G. Cappello, Cell-like pressure sensors reveal increase of mechanical stress towards the core of multicellular spheroids under compression, *Nat. Commun.* 8 (2017) 14056.
- [10] E. Mohagheghian, J. Luo, J. Chen, G. Chaudhary, J. Chen, J. Sun, R.H. Ewoldt, N. Wang, Quantifying compressive forces between living cell layers and within tissues using elastic round microgels, *Nat. Commun.* 9 (1) (2018) 1878.
- [11] W. Lee, N. Kalashnikov, S. Mok, R. Halaoui, E. Kuzmin, A.J. Putnam, S. Takayama, M. Park, L. McCaffrey, R. Zhao, Dispersible hydrogel force sensors reveal patterns of solid mechanical stress in multicellular spheroid cultures, *Nat. Commun.* 10 (1) (2019) 144.
- [12] N. Traeber, K. Uhlmann, S. Girardo, G. Kesavan, K. Wagner, J. Friedrichs, R. Goswami, K. Bai, M. Brand, C. Werner, Polyacrylamide bead sensors for in vivo quantification of cell-scale stress in zebrafish development, *Sci. Rep.* 9 (1) (2019) 1–14.
- [13] D. Vorselen, Y. Wang, M.M. de Jesus, P.K. Shah, M.J. Footer, M. Huse, W. Cai, J. A. Theriot, Microparticle traction force microscopy reveals subcellular force exertion patterns in immune cell-target interactions, *Nat. Commun.* 11 (1) (2020) 20.
- [14] M.K. Shah, I.H. Garcia-Pak, E.M. Darling, Influence of inherent mechanophenotype on competitive cellular adherence, *Ann. Biomed. Eng.* 45 (8) (2017) 2036–2047.
- [15] N.R. Labriola, E. Mathiowitz, E.M. Darling, Fabricating polyacrylamide microbeads by inverse emulsification to mimic the size and elasticity of living cells, *Biomaterials science* 5 (1) (2017) 41–45.
- [16] N.R. Labriola, J.S. Sadick, J.R. Morgan, E. Mathiowitz, E.M. Darling, Cell mimicking microparticles influence the organization, growth, and mechanophenotype of stem cell spheroids, *Ann. Biomed. Eng.* 46 (8) (2018) 1146–1159.
- [17] B.A. Bunnell, M. Flaata, C. Gagliardi, B. Patel, C. Ripoll, Adipose-derived stem cells: isolation, expansion and differentiation, *Methods* 45 (2) (2008) 115–120.
- [18] J.M. Gimble, A.J. Katz, B.A. Bunnell, Adipose-derived stem cells for regenerative medicine, *Circ. Res.* 100 (9) (2007) 1249–1260.
- [19] Y. Zhu, T. Liu, K. Song, X. Fan, X. Ma, Z. Cui, Adipose-derived stem cell: a better stem cell than BMSC, *Cell Biochem. Funct.: Cellular biochemistry and its modulation by active agents or disease* 26 (6) (2008) 664–675.
- [20] R. Dubay, J. Fiering, E. Darling, Effect of elastic modulus on inertial displacement of cell-like particles in microchannels, *Biomicrofluidics* 14 (2020), 0000001.
- [21] E. Darling, S. Zauscher, F. Guilak, Viscoelastic properties of zonal articular chondrocytes measured by atomic force microscopy, *Osteoarthritis Cartilage* 14 (6) (2006) 571–579.
- [22] E. Leary, C. Rhee, B.T. Wilks, J.R. Morgan, Quantitative live-cell confocal imaging of 3D spheroids in a high-throughput format, *SLAS TECHNOLOGY: Translating Life Sciences Innovation* 23 (3) (2018) 231–242.
- [23] M.K. Shah, E.A. Leary, E.M. Darling, Integration of hyper-compliant microparticles into a 3D melanoma tumor model, *J. Biomech.* 82 (2019) 46–53.
- [24] B.T. Estes, B.O. Diekmann, J.M. Gimble, F. Guilak, Isolation of adipose-derived stem cells and their induction to a chondrogenic phenotype, *Nat. Protoc.* 5 (7) (2010) 1294.
- [25] T.J. Hughes, *The Finite Element Method: Linear Static and Dynamic Finite Element Analysis*, Courier Corporation 2012.
- [26] J.E. Frith, B. Thomson, P.G. Genever, Dynamic three-dimensional culture methods enhance mesenchymal stem cell properties and increase therapeutic potential, *Tissue Eng. C Methods* 16 (4) (2010) 735–749.
- [27] R. McBeath, D.M. Pirone, C.M. Nelson, K. Bhadriraju, C.S. Chen, Cell shape, cytoskeletal tension, and RhoA regulate stem cell lineage commitment, *Dev. Cell* 6 (4) (2004) 483–495.
- [28] S. Sart, A.-C. Tsai, Y. Li, T. Ma, Three-dimensional aggregates of mesenchymal stem cells: cellular mechanisms, biological properties, and applications, *Tissue Eng. B Rev.* 20 (5) (2014) 365–380.
- [29] D.M. Dean, A.P. Napolitano, J. Youssef, J.R. Morgan, Rods, tori, and honeycombs: the directed self-assembly of microtissues with prescribed microscale geometries, *Faseb. J.* 21 (14) (2007) 4005–4012.